Subduction II
Fundamentals of Mantle Dynamics

Thorsten W Becker
University of Southern California

Short course at Universita di Roma TRE
April 18 – 20, 2011

Rheology

Elasticity vs. viscous deformation

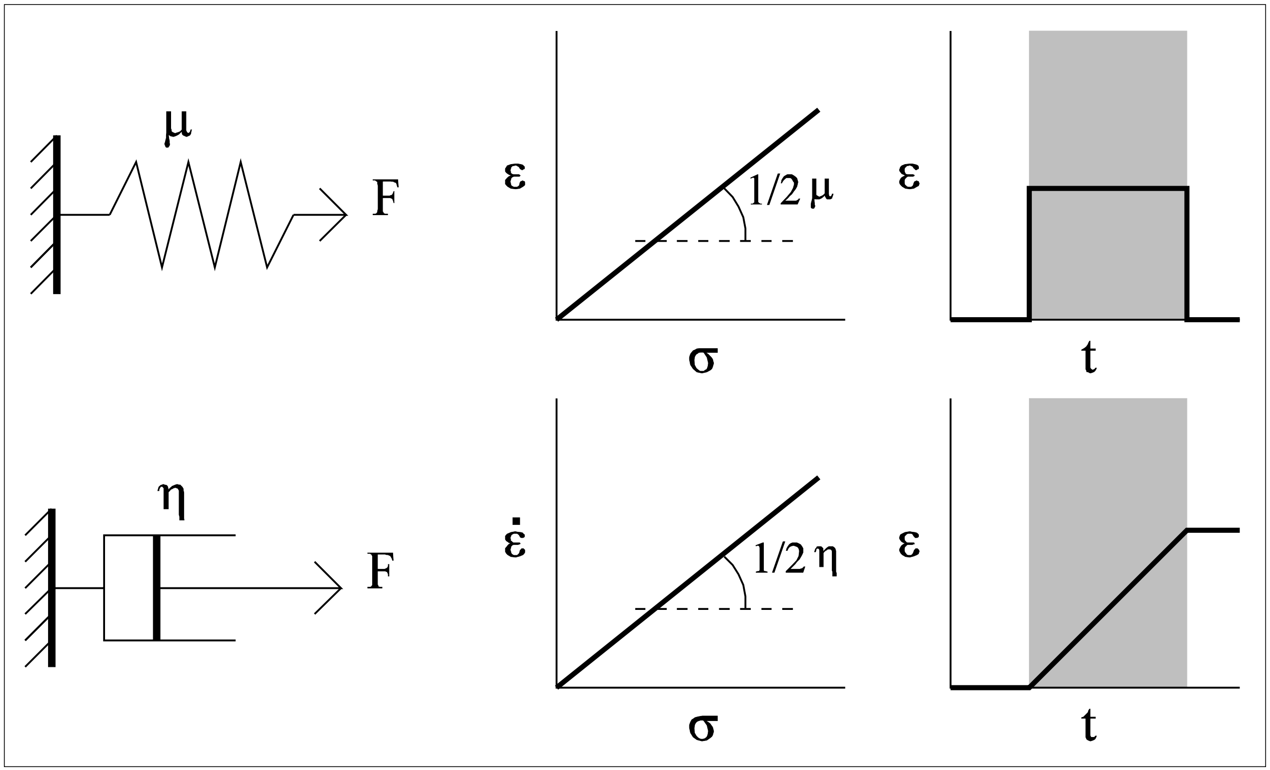

η = O (10^{21}) Pa s = viscosity

μ= O (10^{11}) Pa = shear modulus = rigidity

$\tau = \eta / \mu$ = O(10^{10}) sec = O(10^3) years = Maxwell time

Elastic deformation

In general:

$\sigma_{ij} = C_{ijkl}\, \varepsilon_{kl}$

(in 3-D 81 degrees of freedom, in general 21 independent)

For isotropic body this reduces to Hooke's law:

$\sigma_{ij} = \lambda\varepsilon_{kk}\delta_{ij} + 2\mu\varepsilon_{ij}$

with λ and μ Lame's parameters, $\varepsilon_{kk} = \varepsilon_{11} + \varepsilon_{22} + \varepsilon_{33}$

Taking shear components ($i \neq j$) gives definition of rigidity:

$\sigma_{12} = 2\mu\varepsilon_{12}$

Adding the normal components (*i=j*) for all i=1,2,3 gives:

$\sigma_{kk} = (3\lambda + 2\mu)\, \varepsilon_{kk} = 3\kappa\varepsilon_{kk}$

with $\kappa = \lambda + 2\mu/3$ = bulk modulus

Linear viscous deformation (1)

Total stress field = static + dynamic part:

$$\sigma_{ij} = -p\delta_{ij} + \tau_{ij}$$

Analogous to elasticity …
General case:

$$\tau_{ij} = C'_{ijkl}\,\dot{\varepsilon}_{kl}$$

Isotropic case:

$$\tau_{ij} = \lambda'\dot{\varepsilon}_{kk}\delta_{ij} + 2\eta\dot{\varepsilon}_{ij}$$

Linear viscous deformation (2)

Split in isotropic and deviatoric part (latter causes deformation):

$$\sigma'_{ij} = \sigma_{ij} - \frac{1}{3}\sigma_{kk}\delta_{ij} = \sigma_{ij} + \bar{p}\delta_{ij}$$

$$\dot{\varepsilon}'_{ij} = \dot{\varepsilon}_{ij} - \frac{1}{3}\dot{\varepsilon}_{kk}\delta_{ij}$$

which gives the following stress:

$$\sigma'_{ij} = (\bar{p} - p)\delta_{ij} + \varsigma\dot{\varepsilon}_{kk}\delta_{ij} + 2\eta\dot{\varepsilon}'_{ij}$$

With compressibility term assumed 0 (Stokes condition $\dot{\varepsilon}_{kk} = 0$)

($\varsigma = \lambda' + \frac{2}{3}\eta =$ bulk viscosity)

Now $\tau_{ij} = 2\eta\dot{\varepsilon}_{ij}$ or $\eta = \dfrac{\tau_{ij}}{2\dot{\varepsilon}_{ij}}$

In general $\eta = f(T, d, p, H_2O)$

Non-linear (or non-Newtonian) deformation

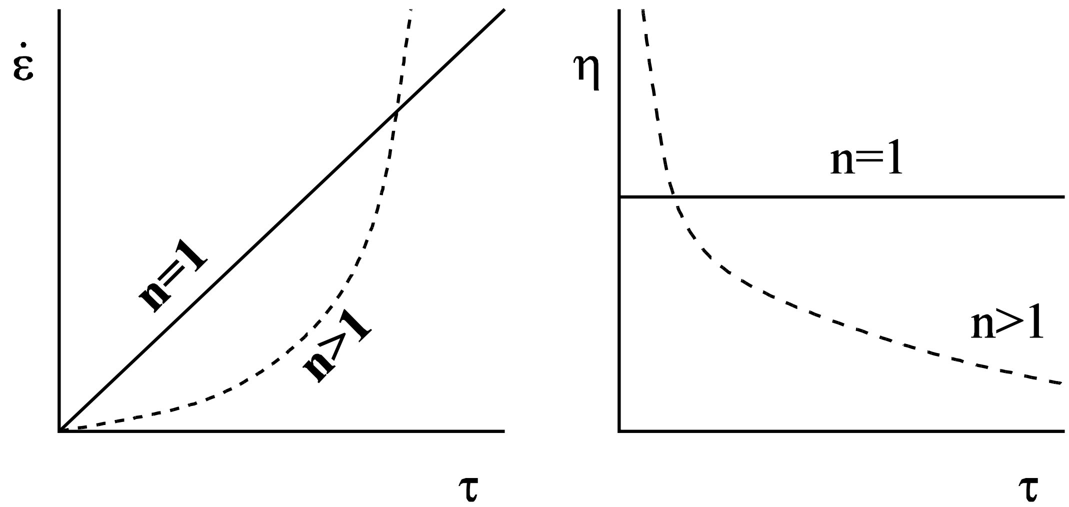

General stress-strain relation: $\dot{\varepsilon} = A\tau^n$

$n = 1$: Newtonian

$n > 1$: non-Newtonian

$n \rightarrow \infty$: pseudo-brittle

Effective viscosity $\eta_{eff} = \frac{1}{2} A^{-1} \tau^{1-n} = \frac{1}{2} A^{-1/n} \dot{\varepsilon}^{(1-n)/n}$

Application: different viscosities under oceans with different absolute plate motion, anisotropic viscosities by means of superposition (Schmeling, 1987)

Microphysical theory and observations
Maximum strength of materials (1)

'Strength' is maximum stress that material can resist
In principle, viscous fluid has zero strength.
In reality, all materials have finite strength.

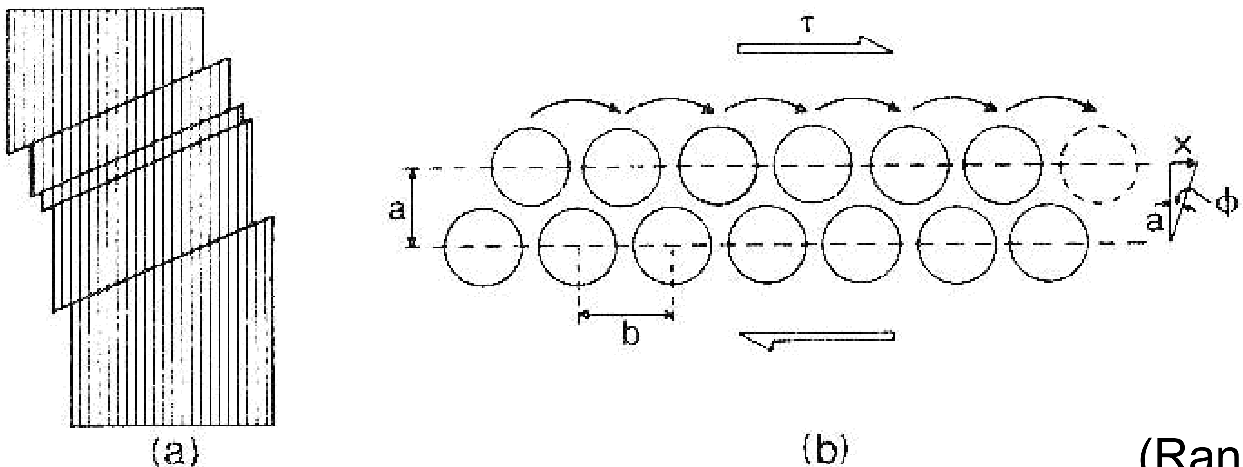

(Ranalli, 1995)

Elastic deformation until atom jumps to next equilibrium position.

So theoretical strength $\sigma = O(\mu)$

Microphysical theory and observations
Maximum strength of materials (2)

However, from laboratory measurements:

Shear strength $= O(10^{-4}\mu)$ due to:

- Structural flaws
- Cracks
- Vacancies
- Dislocations
- Subgrain boundaries

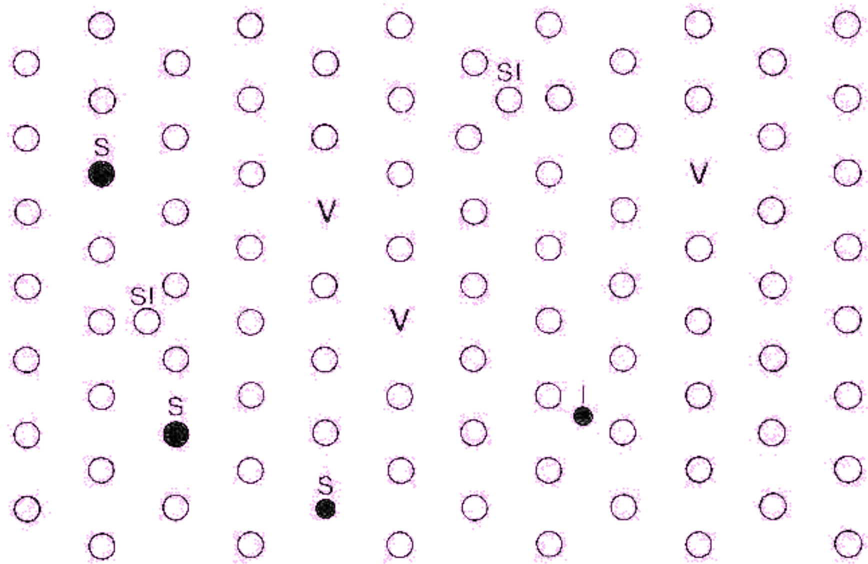

Figure 9.4 Point defects in crystals (open circles denote atoms occupying the nodes of the lattice): V, vacancies; SI, self-interstitials; S, substitutional impurities; I, interstitial impurities.

(Ranalli, 1995)

Stress concentration makes deformation possible under smaller stresses (compare to breaking/tearing of sheet of paper)

Diffusion creep

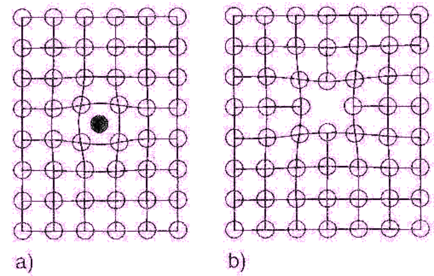

Figure 5.16. Point defects in a crystal lattice. (a) An interstitial or extra atom, (b) a vacancy. The lattice tends to distort around the defect. After Twiss and Moores (1992).

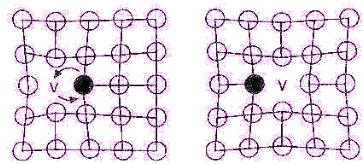

Figure 5.17. Illustration of the motion of a vacancy (v) from one lattice site to an adjacent one by the opposite motion of an atom (solid circle). Matter and vacancies diffuse in opposite directions. After Twiss and Moores (1992).

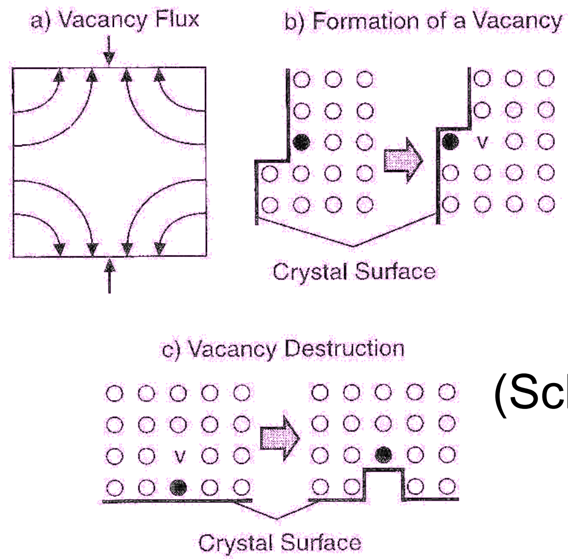

(Schubert, Turcotte & Olson, 2001)

Figure 5.18. Diffusion creep or Herring-Nabarro creep due to vacancy diffusion in a crystal under uniaxial compression. (a) Vacancies diffuse toward the surface of highest normal (compressive) stress along the indicated paths. Atoms diffuse in the opposite direction. (b) Creation of a vacancy at a surface of minimum compressive stress. The solid lines mark the crystal surface. The solid circle marks the ion whose position changes to create the vacancy (v). The surface gradually builds out, lengthening the crystal normal to the compressive stress. Vacancies diffuse toward a surface of high compressive stress. (c) Destruction of a vacancy at a surface of maximum compressive stress. Removal of atoms from the surface and destruction of vacancies gradually shortens the crystal parallel to the maximum compressive stress. After Twiss and Moores (1992).

Dislocation creep

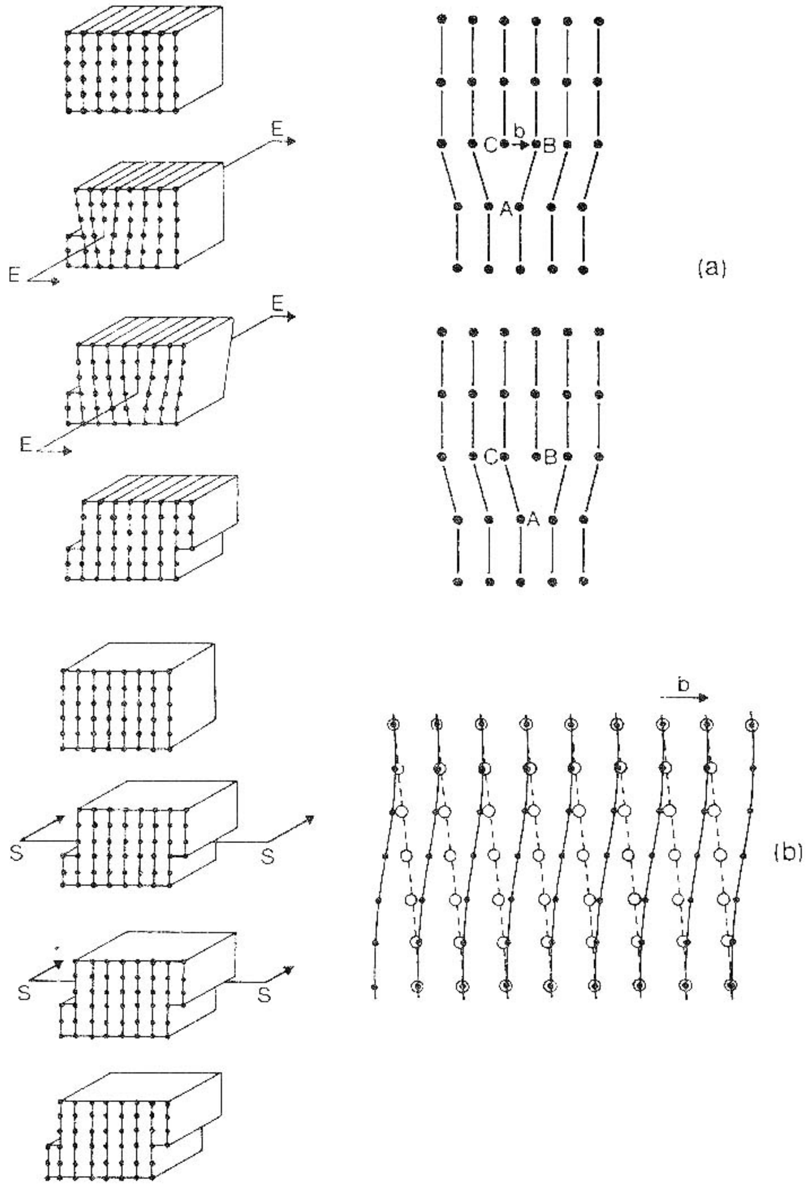

Figure 9.6 (a) Slip by propagation of an edge dislocation EE, equivalent to an extra half-plane in the lattice; (b) slip by propagation of a screw dislocation SS, with atoms forming a helix around the dislocation line. (Representations of slip and of atomic arrangement of edge dislocation from Nicolas & Poirier 1976. Atomic arrangement of screw dislocation reproduced from Hull 1975.)

(Ranalli, 1995)

Steady state creep models

Theoretically many different models: only a few relevant for Earth

• (Climb-controlled) dislocation creep or *powerlaw* creep: gliding of dislocations controlled by the climb rate around impurities/obstacles:

$$\dot{\epsilon} \propto D_{SD} \left(\frac{\sigma}{\mu} \right)^{n} \qquad D_{SD} = D_0 \exp\left(-\frac{E^{¿} + pV^{¿}}{RT} \right)$$

• Diffusion creep (Newtonian, linear creep):

- Nabarro-Herring creep (diffusion through grain)
- Coble creep (diffusion along grain boundary)

$$\dot{\epsilon} \propto \frac{D_{SD}}{d^{m}} \left(\frac{\sigma}{\mu} \right)$$

m=2-3

• Peierl's stress mechanism (low-T plasticity): dislocation glide
• Grain-boundary sliding (superplasticity)
• Pressure-solution
• Brittle deformation, Byerlee's 'law'

Strength of the Lithosphere and Mantle

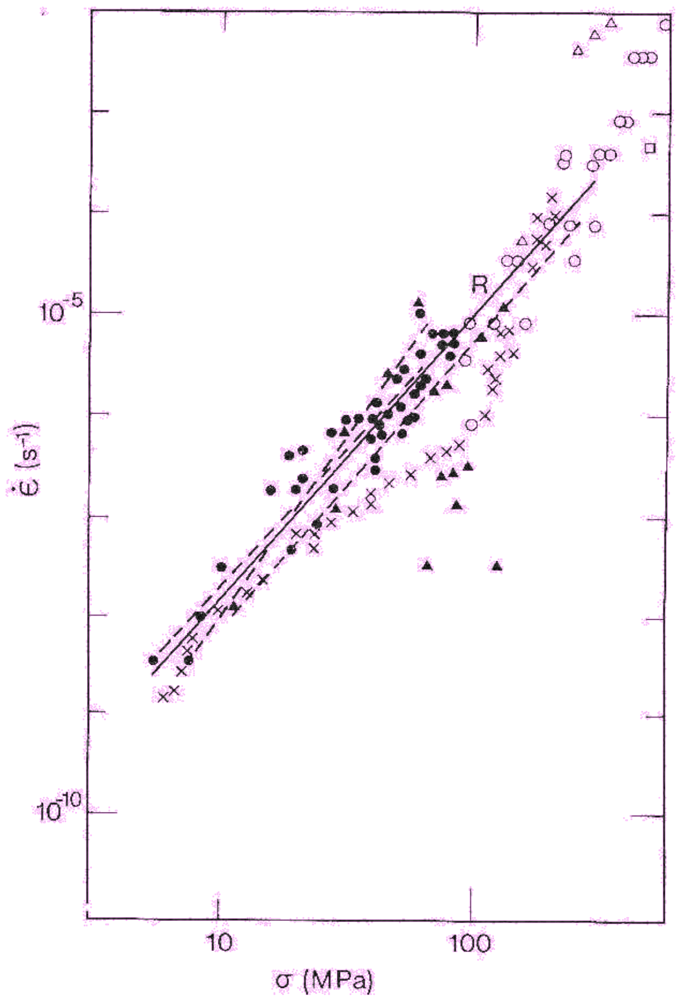

Figure 10.10 Experimental stress–strain rate diagram for olivine (data from various sources). Continuous line (R) gives the fit to the data provided by the theoretical power-law creep equation (from Ranalli 1982).

Experimental data for olivine

Strength of the Lithosphere and Mantle

TABLE 7–5 **Parameter Values for Diffusion Creep and Dislocation Creep in a Dry Upper Mantle (Karato and Wu, 1993)***

Quantity	**Diffusion Creep**	**Dislocation Creep**
Preexponential factor A, s^{-1}	8.7×10^{15}	3.5×10^{22}
Stress exponent n	1	3.5
Grain size exponent m	2.5	0
Activation energy E_a, kJ mol^{-1}	300	540
Activation volume V_a, m^3 mol^{-1}	6×10^{-6}	2×10^{-5}

* Other relevant parameter values are $G = 80$ GPa, $b = 0.5$ nm, and $R = 8.3144$ J K^{-1} mol^{-1}.

TABLE 7–4 **Rheological Parameter Values of Geologic Materials**

Material	**C_1 (MPa^{-n} S^{-1})**	**n**	**E_a (kJ mol^{-1})**
Ice	8.8×10^5	3	60.7
Halite	9.5×10^{-1}	5.5	98.3
Dry quartzite	6.7×10^{-12}	6.5	268
Wet quartzite	4.4×10^{-2}	2.6	230
Limestone	4.0×10^3	2.1	210
Maryland diabase	5.2×10^2	3	356

(Turcotte and Schubert, 2002)

Collection of rheological data for different materials

$$\dot{e} = A\sigma^n d^{-m} C^r_{H_20} \exp(-\alpha\phi) \exp\left(-\frac{E+pV}{RT}\right)$$

$$\dot{\varepsilon} = A''\tau^n d^{-m} \exp\left(-\frac{E+pV}{RT}\right)$$

$$A'' = \frac{3^{\frac{n+1}{2}}}{2^{1-n}} 10^{-6(m+n)} C^r_{H_20} A$$

type	A eq. (1) Hirth & Kohlstedt (2004) units	A'' eq. (3) SI units	n	m	E [kJ/mol]	V $[10^{-6}\mathrm{m}^3/\mathrm{mol}]$
		diffusion creep				
dry	1.5×10^9	4.5×10^{-15}	1	3	375	6
wet	10^5	3.0×10^{-15}	1	3	335	4
		dislocation creep				
dry	1.1×10^5	7.4×10^{-15}	3.5	0	530	14
wet	90	2.4×10^{-14}	3.5	0	480	11

See Hirth & Kohlstedt (2005)
for olivine in the upper mantle

Laboratory experiments: large temperature, strain-rate & grain-size dependence.

- Viscous flow law (for each mechanism):

$$\eta = \left(\frac{d^p}{A e^{(a\phi)} C_{OH}^r} \right)^{\frac{1}{n}} \dot{\epsilon}_{II}^{\frac{1-n}{n}} \exp\left[\frac{E + P_{lc} V}{n R T_t} \right]$$

where,
$T_t = T + T_{ad}$.
P_{lc} is the lithostatic pressure, including a compressibility gradient.

For dislocation (ds) creep $p = 0$, $n = 3.5$.
For diffusion (df) creep $p = 3$, $n = 1$.

- Dislocation (ds) & diffusion (df) creep accommodate total strain-rate:

$$\dot{\epsilon} = \dot{\epsilon}_{df} + \dot{\epsilon}_{ds} \tag{2}$$

- For deformation at constant stress, the effective viscosity is:

$$\eta_{ef} = \frac{\eta_{df}\eta_{ds}}{\eta_{df} + \eta_{ds}} \tag{3}$$

For a background upper mantle viscosity of $\eta_o = 10^{20}$ Pas (at 250 km):
– Transition strain-rate ($\dot{\epsilon}_{df} = \dot{\epsilon}_{ds}$): $\dot{\epsilon}_t = 10^{-15}\ \mathrm{s}^{-1}$
for $C_{OH} = 300$ ppm-H/Si & $d = 10$ mm.

Dislocation creep decreases viscosity where the strain-rate is more than the transition value.

- Plastic yield stress, σ_y, limits the stress (and viscosity). If,

$$\sigma_y > \eta_{df}\dot{\epsilon}_{II}$$

then,

$$\eta_y = \sigma_y/\dot{\epsilon}_{II}$$

- Composite viscosity:

$$\eta_{comp} = \min(\eta_{ef}, \eta_y)$$

- ***Non-deforming regions remain highly viscous.***
- ***Yielding concentrates deformation.***

Deformation maps

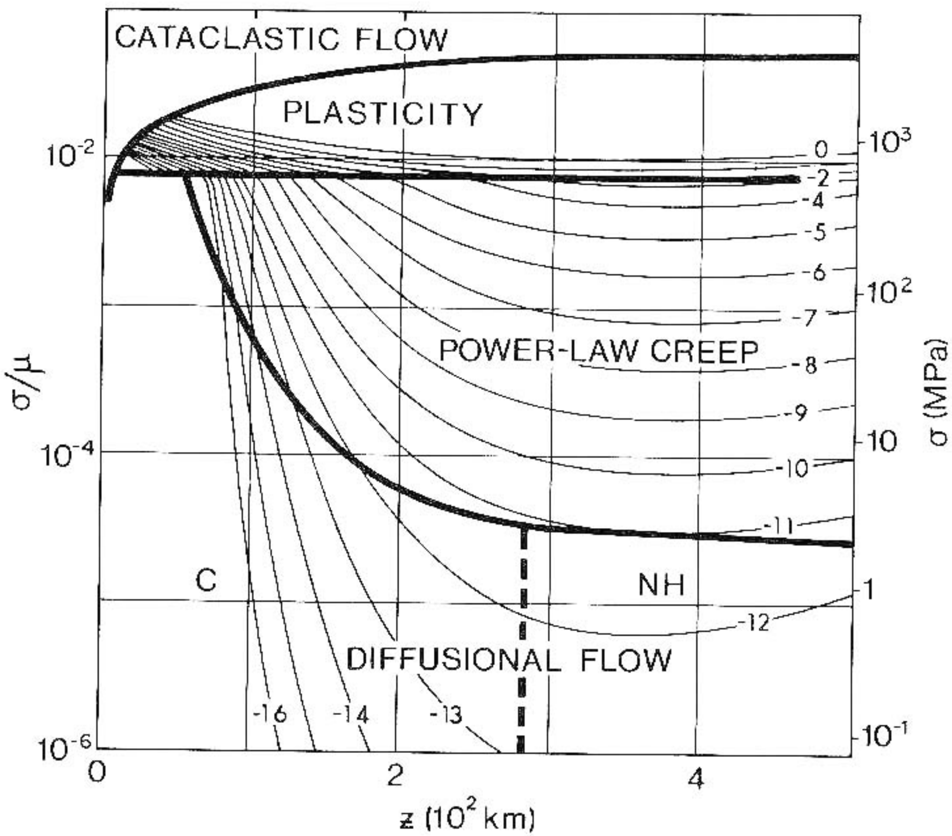

Figure 11.1 (σ, z)-deformation map for polycrystalline olivine with grain size 0.1 mm. Thick lines are creep field boundaries; thin lines, constant strain rate contours (given as powers of 10). C and NH denote Coble and Nabarro–Herring creep, respectively (from Ashby and Verrall 1978).

(Ranalli, 1995)

Strength of the Lithosphere and Mantle (3)

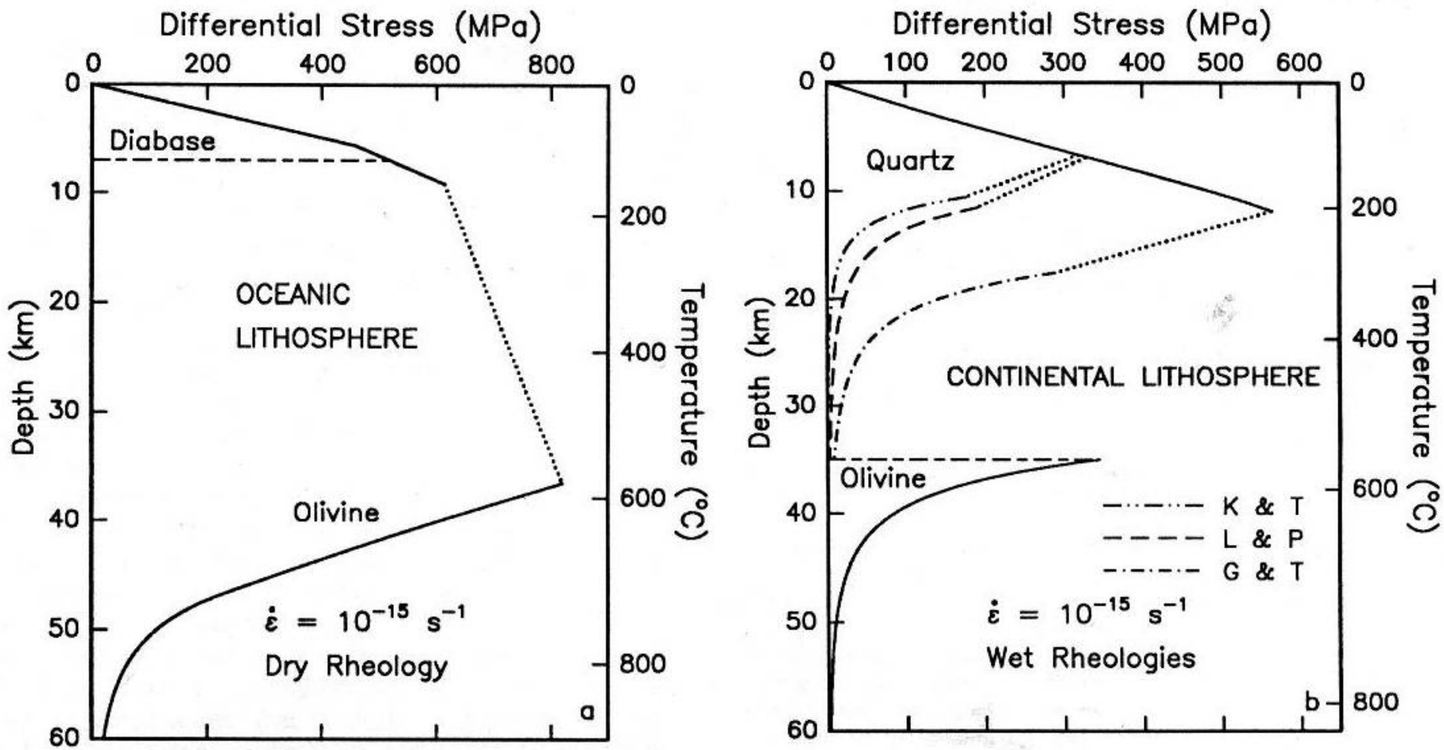

Figure 9. Strength envelopes for oceanic and continental lithosphere. (a) For the oceanic lithosphere, a geotherm for 60-m.y.-old lithosphere was used [e.g., *Turcotte and Schubert*, 1982 pp. 163-167]. A rheology for dry olivine [*Chopra and Paterson*, 1984] was used because water strongly partitions into the melt during partial melting. (b) For the continental lithosphere, a geotherm for a surface heat flow of 60 mW m^{-1} was employed [*Chapman*, 1986]. The rheologies for wet quartzite are those used in Figure 5; the olivine rheology is for wet Anita Bay dunite from *Chopra and Paterson* [1984]. Wet rheologies were used, consistent with high fluid pressures in fault zones. Plastic flow strength was corrected for water fugacity using a water fugacity exponent of unity and assuming lithostatic pore pressure. The BDT and BPT, determined as described in the text, have been connected by a dotted line.

(Kohlstedt et al., 1995) Strength curves for different materials: lithosphere

Slab rheology

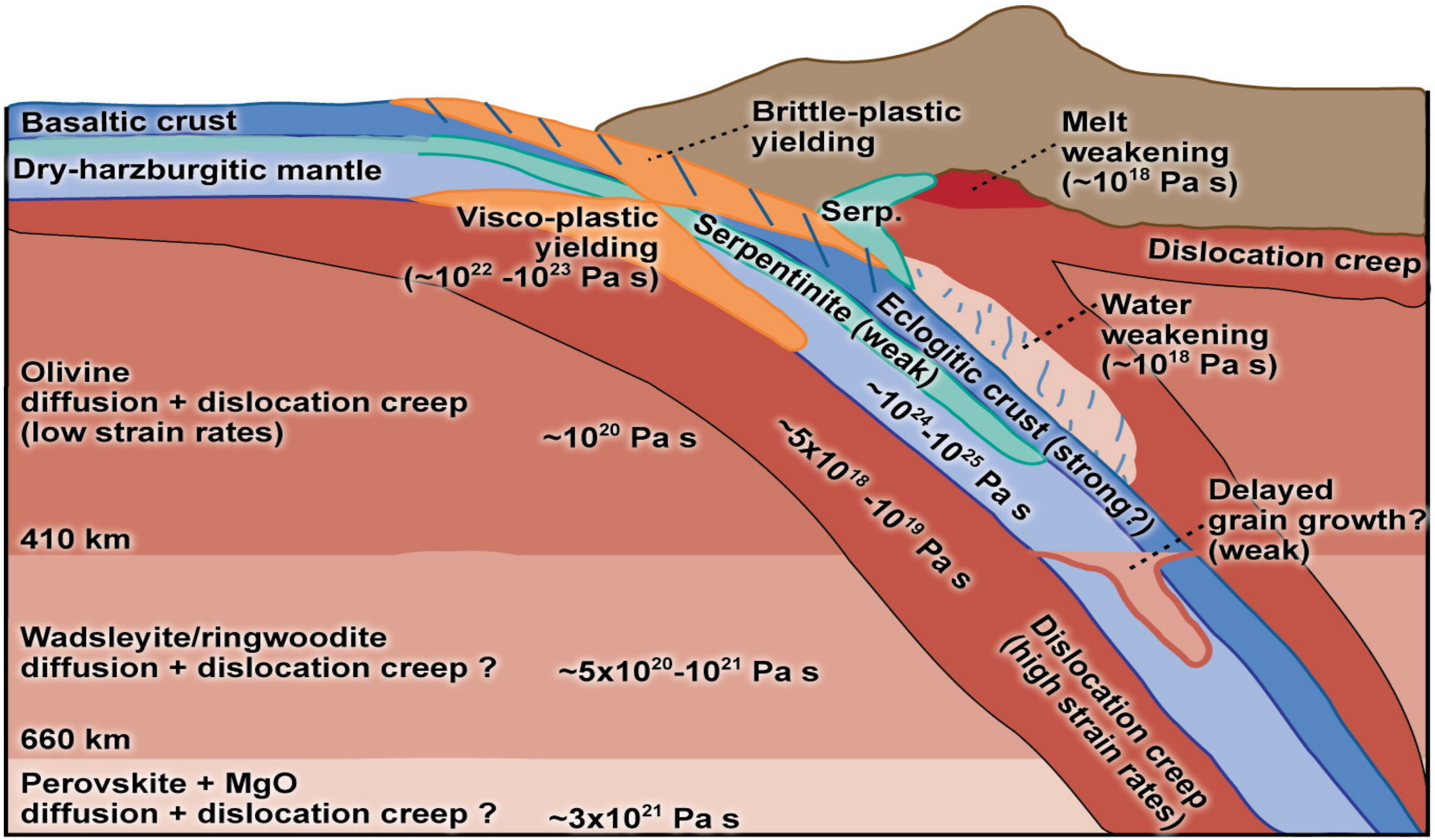

Billen MI. 2008.
Annu. Rev. Earth Planet. Sci. 36:325–56.

Figure courtesy of M. Billen

Governing equations

- Conservation of mass: continuity
- Conservation of momentum: Stokes' equation
- Equation of state: density
- constitutive equation: rheology
- Conservation of energy: temperature

Continuity

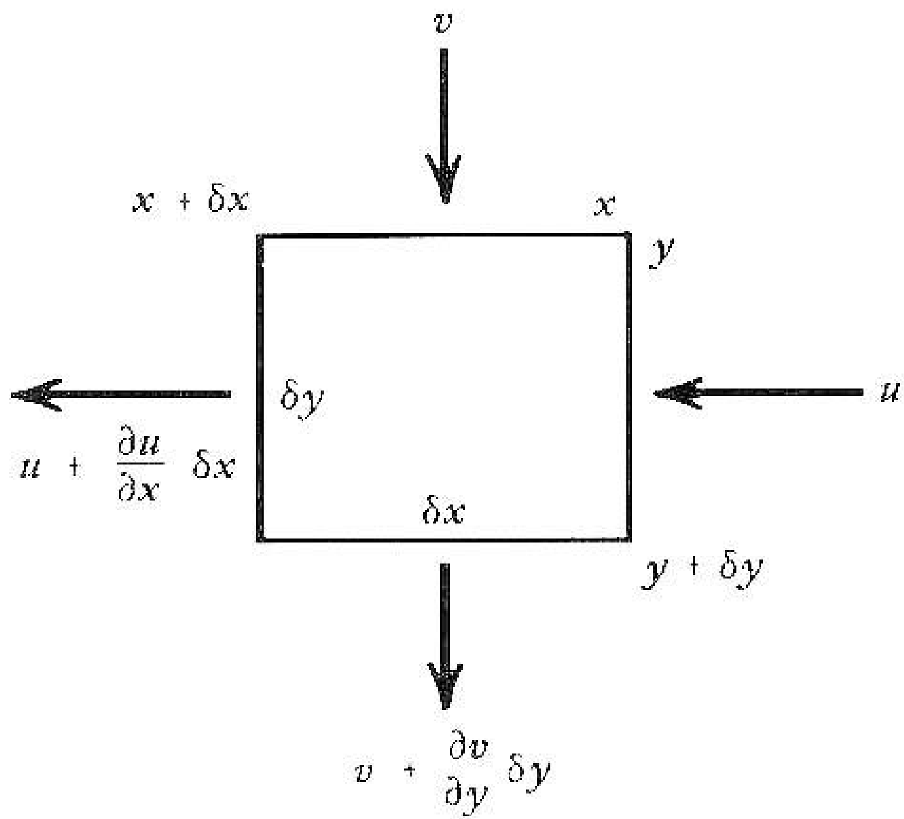

(from Turcotte and Schubert, 2002)

This gives: $\nabla \cdot u = 0$

Derivation of Stokes equation

Static force balance

$$\nabla \cdot \sigma + \vec{f} = \vec{0} \qquad \frac{\partial \sigma_{ij}}{\partial x_j} + f_i = 0$$

Incompressible constitutive relationship and separation into deviatoric stress

$$\sigma_{ij} = \tau_{ij} - p\,\delta_{ij} = 2\eta\,\dot{\epsilon}_{ij} - p\,\delta_{ij}$$

Constant viscosity

$$2\eta \frac{\partial \dot{\epsilon}_{ij}}{\partial x_j} - \frac{\partial p}{\partial x_i} + f_i = 0$$

Derivation of Stokes equation (2)

$$2\frac{\partial \dot{\epsilon}_{ij}}{\partial x_j} = \frac{\partial}{\partial x_j}\left(\frac{\partial v_i}{\partial x_j} + \frac{\partial v_j}{\partial x_i}\right) = \frac{\partial^2 v_i}{\partial x_j x_j} + \frac{\partial}{\partial x_i}\left(\frac{\partial v_j}{\partial x_j}\right)$$

$$2\frac{\partial \dot{\epsilon}_{ij}}{\partial x_j} = \frac{\partial^2 v_i}{\partial x_j \partial x_j} = \nabla^2 v_i$$

Because for incompressible

$$\frac{\partial v_j}{\partial x_j} = 0$$

$$\eta \nabla^2 v_i - \frac{\partial p}{\partial x_i} + f_i = 0$$

$$\eta \nabla^2 \vec{v} - \vec{\nabla} p + \vec{f} = \vec{0}$$

$$\eta \frac{\partial^2 v_i}{\partial x_j \partial x_j} - \frac{\partial p}{\partial x_i} + f_i = 0$$

Incompressible, Newtonian flow

$$\rho\left(\frac{\partial \mathbf{v}}{\partial t}+\mathbf{v}\cdot\nabla\mathbf{v}\right)=-\nabla p+\mu\nabla^2\mathbf{v}+\mathbf{f}.$$

$$\rho\left(\frac{\partial u}{\partial t}+u\frac{\partial u}{\partial x}+v\frac{\partial u}{\partial y}+w\frac{\partial u}{\partial z}\right)=-\frac{\partial p}{\partial x}+\mu\left(\frac{\partial^2 u}{\partial x^2}+\frac{\partial^2 u}{\partial y^2}+\frac{\partial^2 u}{\partial z^2}\right)+\rho g_x$$

$$\rho\left(\frac{\partial v}{\partial t}+u\frac{\partial v}{\partial x}+v\frac{\partial v}{\partial y}+w\frac{\partial v}{\partial z}\right)=-\frac{\partial p}{\partial y}+\mu\left(\frac{\partial^2 v}{\partial x^2}+\frac{\partial^2 v}{\partial y^2}+\frac{\partial^2 v}{\partial z^2}\right)+\rho g_y$$

$$\rho\left(\frac{\partial w}{\partial t}+u\frac{\partial w}{\partial x}+v\frac{\partial w}{\partial y}+w\frac{\partial w}{\partial z}\right)=-\frac{\partial p}{\partial z}+\mu\left(\frac{\partial^2 w}{\partial x^2}+\frac{\partial^2 w}{\partial y^2}+\frac{\partial^2 w}{\partial z^2}\right)+\rho g_z$$

– Conservation of Mass:

$$\frac{\partial \rho}{\partial t} + \nabla \cdot \rho \vec{v} = 0$$

– Conservation of Momentum:

$$\rho \left(\frac{\partial \vec{v}}{\partial t} + (\vec{v} \cdot \nabla) \vec{v} \right) = \nabla \cdot \vec{\sigma} - g \rho \vec{z}$$

– Conservation of Energy:

$$\frac{\partial C_p T}{\partial t} + \vec{v} \cdot \nabla C_p T = \frac{1}{\rho} \nabla \cdot k \nabla T + H$$

– Conservation of Mass (incompressible; $\delta\rho = 0$):

$$\nabla \cdot \vec{v} = 0$$

– Boussinesq Approximation ($\delta\rho << \rho$):

$$\rho = \rho_o(1 - \alpha(T - T_o))$$

– Constituitive Equation (incompressible):

$$\sigma_{ij} = \eta \left(\frac{\partial v_i}{\partial x_j} + \frac{\partial v_j}{\partial x_i} \right) - p\delta_{ij}$$

Simplified equations

– Conservation of Mass (incompressible; $\delta\rho = 0$):

$$\nabla \cdot \vec{v} = 0$$

– Conservation of Momentum:

$$\rho\left(\frac{\partial \vec{v}}{\partial t} + (\vec{v}\cdot\nabla)\vec{v}\right) = \eta\nabla^2\vec{v} - \nabla p - g\rho\vec{z}$$

– Conservation of Energy (constant C_p, κ; $H = 0$):

$$\rho\left(\frac{\partial T}{\partial t} + \vec{v}\cdot\nabla T\right) = \kappa\nabla^2 T + \frac{H}{C_p}$$

Simple 1-D fluid dynamics examples

Couette channel flow:

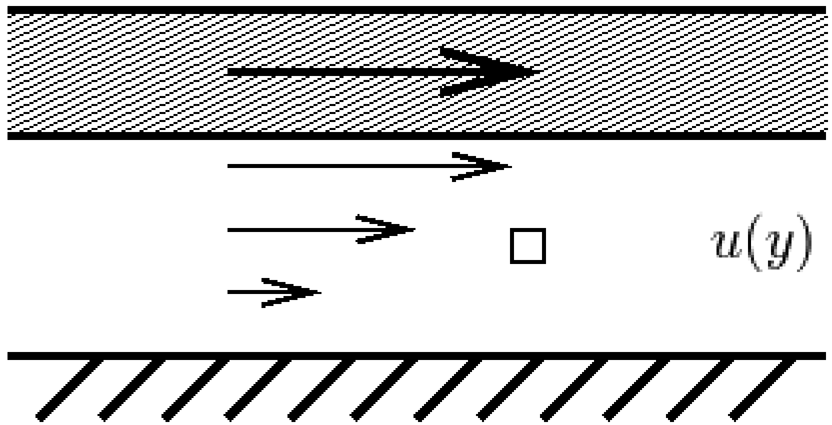

$$u(y) = u_0 \frac{y}{h}$$

$$u(y) = u_0 \frac{y}{h} + \frac{1}{2\mu}\left(\frac{dp}{dx}\right)\left(y^2 - hy\right).$$

Channel flow with horizontal pressure gradient (Hagen Poiseuille):

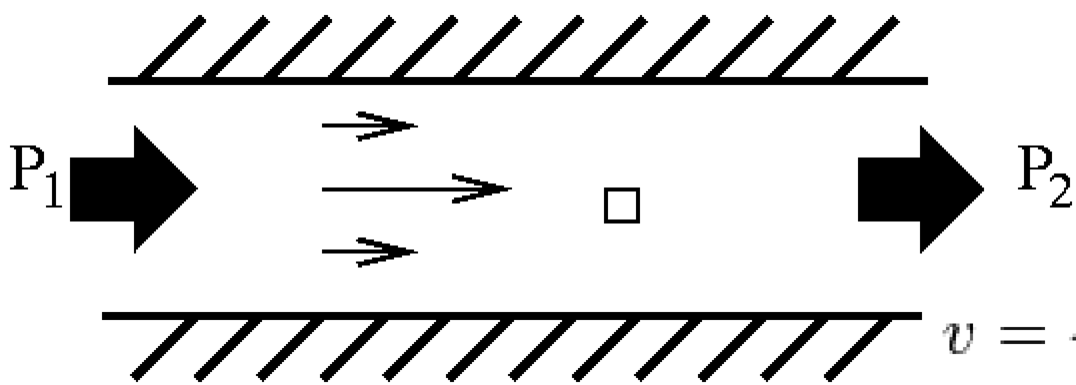

$$v = -\frac{1}{4\eta}\frac{\Delta P}{\Delta x}(R^2 - r^2)$$

Stokes sinker solution

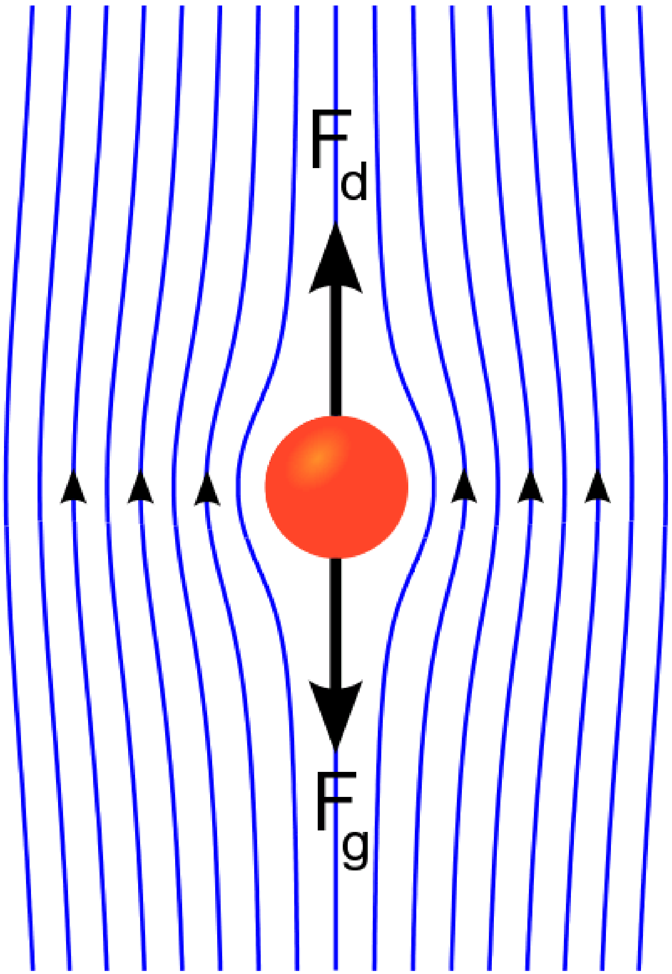

$$V_{\text{Stokes}} = C\frac{\Delta\rho g a^2}{\eta_m}$$

$$C = \frac{2+2\eta'}{6+9\eta'} \qquad \eta' = \frac{\eta_s}{\eta_m}$$

Inferences based on Stokes flow

$$u \propto \frac{\Delta \rho}{\eta}$$

$$\tau \propto \eta \dot{\epsilon} \propto \eta \frac{u}{L} \propto \frac{\Delta \rho}{L}$$

Scaling:

Dimensional equations:

$$\nabla \cdot u = 0$$

$$-\nabla \Delta p + \eta \nabla^2 u = \rho_0 \alpha (T - T_0) g \delta_{i3}$$

$$\rho_0 C_p \frac{dT}{dt} = k \nabla^2 T - \rho C_p \vec{u} \cdot \nabla T$$

Scaling parameters

$$x' = x / h$$

$$t' = t / (h^2 / \kappa)$$

$$T' = (T - T_0) / \Delta T$$

$$\eta' = \eta / \eta_0$$

Scaled equations (with primes left out):

$$\nabla \cdot u = 0$$

$$-\nabla \Delta p + \eta \nabla^2 u = Ra T \delta_{i3}$$ with Rayleigh number $Ra = \frac{\alpha \rho_0 g \Delta T h^3}{\eta \kappa}$

$$\frac{dT}{dt} = \nabla^2 T - \vec{u} \cdot \nabla T$$

Rayleigh numbers

Bottom heated

$$Ra = \frac{\alpha \rho_0 g \Delta T h^3}{\eta \kappa}$$

Internal heating

$$H\, h^3 = k \nabla T\, h^2 = k\, \Delta T\, h$$

$$\Delta T = \frac{H\, h^2}{k}$$

$$Ra_H = \frac{\alpha\, \rho_0\, g\, H\, h^5}{k\, \eta\, \kappa}$$

Effect of phase transitions

Clapeyron slope

$$\gamma = \left(\frac{dp}{dT}\right)_c = \frac{Q_{latent}\,\rho_1\,\rho_2}{T_a\,\Delta\rho}$$

$$Ra = \frac{\alpha\,\rho_0\,g\,\Delta T\,h^3}{\eta\,\kappa} \qquad Rb = \frac{\Delta\rho\,g\,T\,h^3}{\eta\,\kappa}$$

Buoyancy parameter

$$P = \frac{\gamma\,\Delta\rho}{\alpha\,\rho^2\,g\,h} = \frac{Rb}{Ra}\,\bar{\gamma} \qquad \bar{\gamma} = \frac{\gamma}{\gamma_c} \qquad \gamma_c = \frac{\rho_0\,g\,h}{\Delta T}$$

e.g. Schubert et al. (1975); Christensen (1985); Schubert et al. (2001), p. 466f

Linear stability analysis (1)

- for small ΔT (or Ra): conduction
- for larger Ra: convection sets in

→ so minimum Ra = Ra_c exists below which no convection occurs

- $T = T_{conductive} + T_1 = T_0 + T_1$
- For small velocity and T_1 we can linearize system: 'linear stability analysis'

- Energy equation in terms of T_1 and Ψ
- Remove 'small' terms
- Solve with separation of variables:

$$\Psi = \Psi^* \cos(n\pi z)\sin(kx)\exp(\alpha t)$$

$$T_1 = T_1^* \cos(n\pi z)\cos(kx)\exp(\alpha t)$$

- $\alpha<0$: stable
- $\alpha>0$: instable
- $\alpha=0$: marginal stability

$$\boxed{Ra_c = \frac{\left(k^2 n^2 \pi^2\right)^3}{k^2}}$$

See Schubert et al. (2001) p. 288ff

Linear stability analysis (2)

minimum Ra_c = 657.5 for free-slip, bottom heated, λ_c = 2.8

Ra_c as function of horizontal wavelength $k=2\pi b/\lambda$, b = box height, *i.e.*

one wavelength of counter-rotating cells with aspect ratio 2.8 x 1 for $\lambda = \lambda_c$

(from Turcotte and Schubert, 2002)

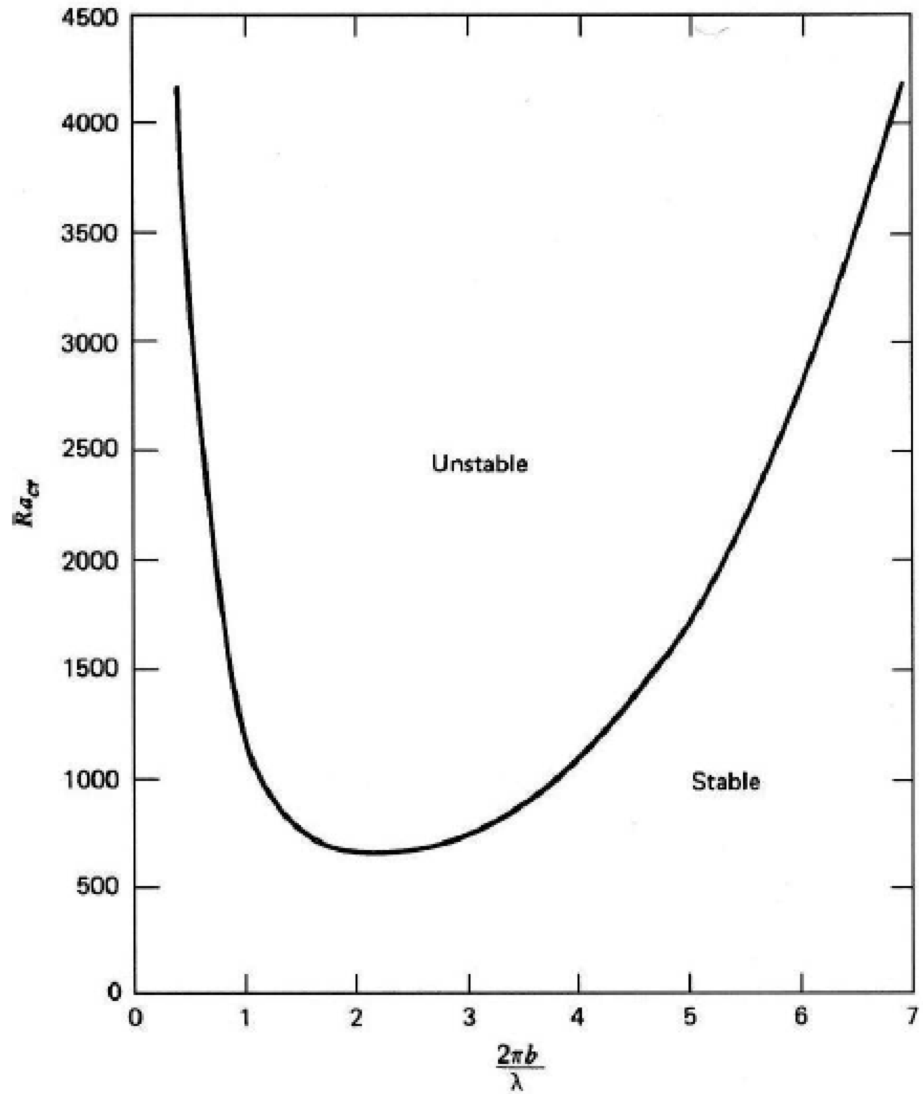

Simple convection model for high Ra

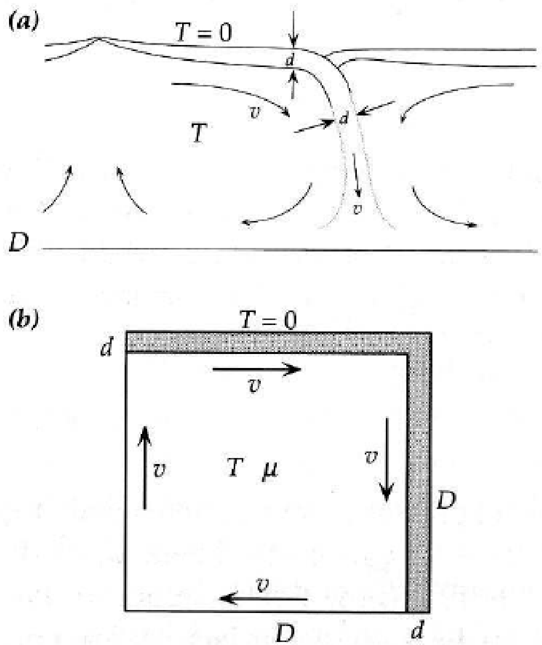

Figure 8.1. (a) Sketch of flow driven by a subducting plate. (b) Idealised form of the situation in (a).

(from (Davies, 1999))

- $B = gDd\rho\alpha\Delta T$
- $R = 4\eta v$
- $R + B = 0$
- $v \sim 14$ cm/yr
- relates physical quantities

Boundary layer theory

$$\frac{T_i - T(x,z)}{T_i - T_0} = \mathrm{erfc}\left[\frac{z}{2}\left(\frac{u}{\kappa x}\right)^{1/2}\right]$$

$$u \propto \frac{\kappa}{h} Ra^{\frac{2}{3}}$$

$$Q \propto \Delta T \, Ra^{\frac{1}{3}}$$

$$Nu \propto Ra^{\frac{1}{3}}$$

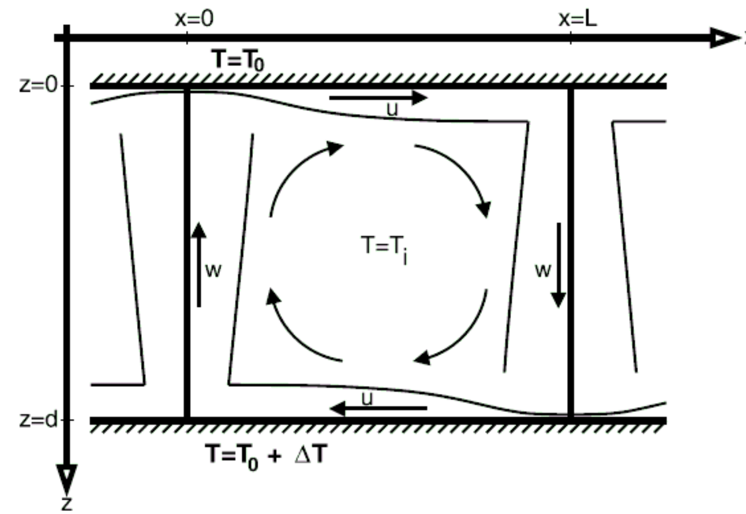

Figure 3. Loop model for a convective cell of width L and height d [from *Turcotte and Oxburgh*, 1967](with permission from Cambridge University Press).

See Schubert et al. (2001) p. 353ff
Grigne et al. (2005)

Example: Boussinesq convection, isoviscous, no internal heating

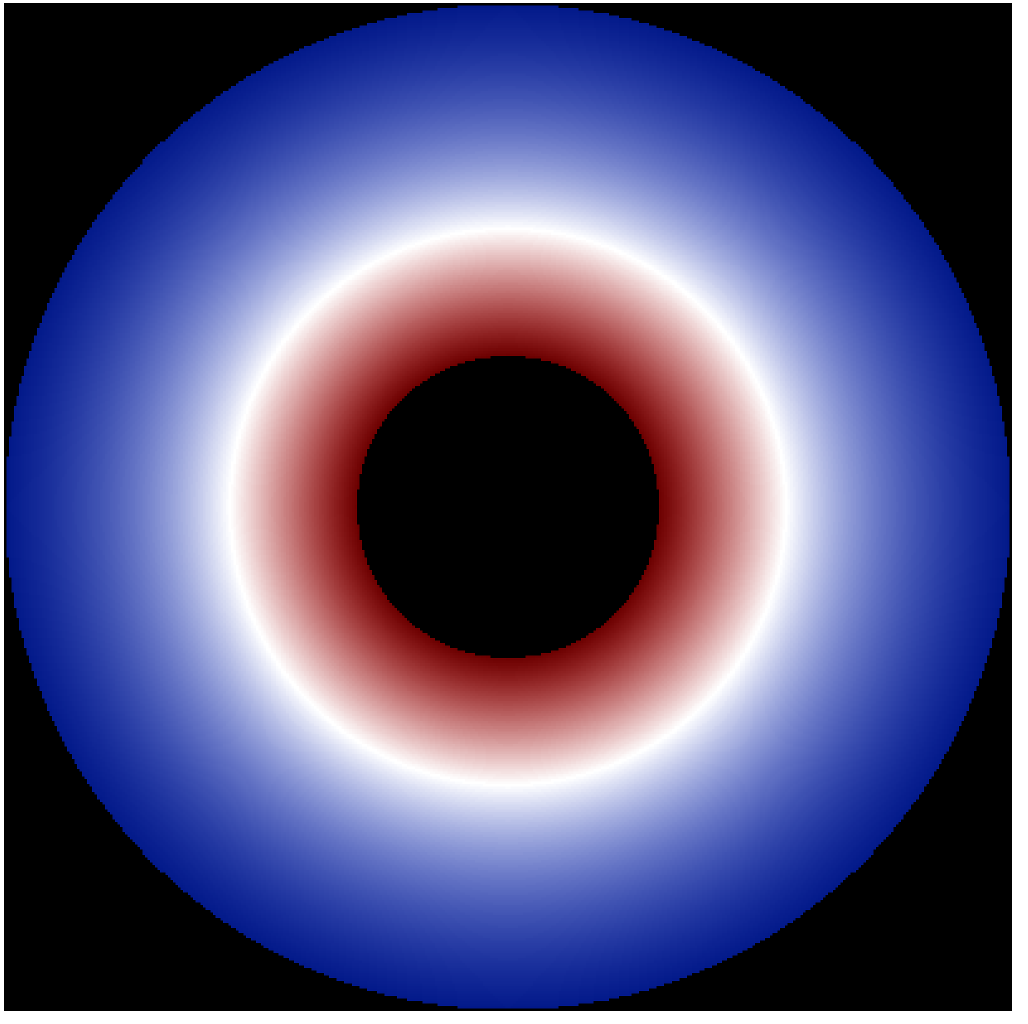

Ra=1 **Nu=1**

Figure courtesy of P. van Keken

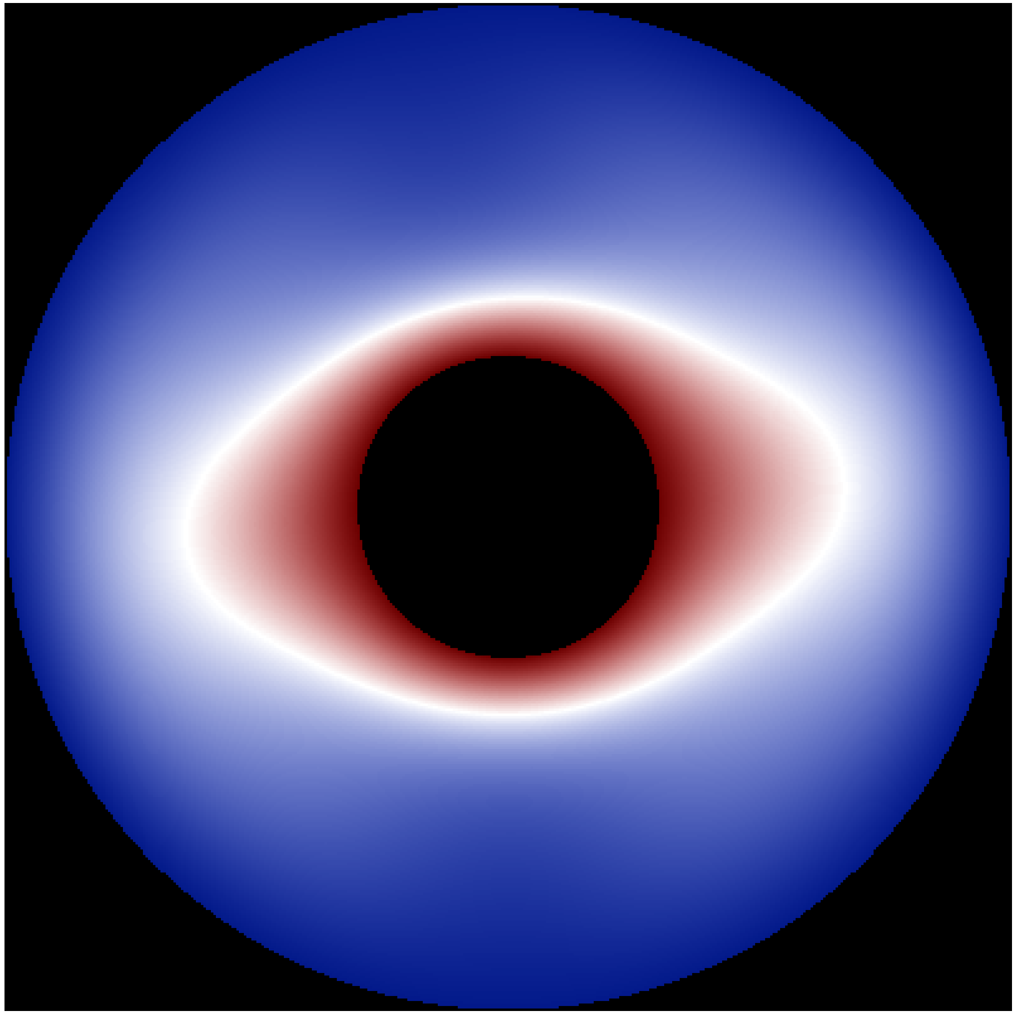

Ra=10^3 **Nu>1**

Figure courtesy of P. van Keken

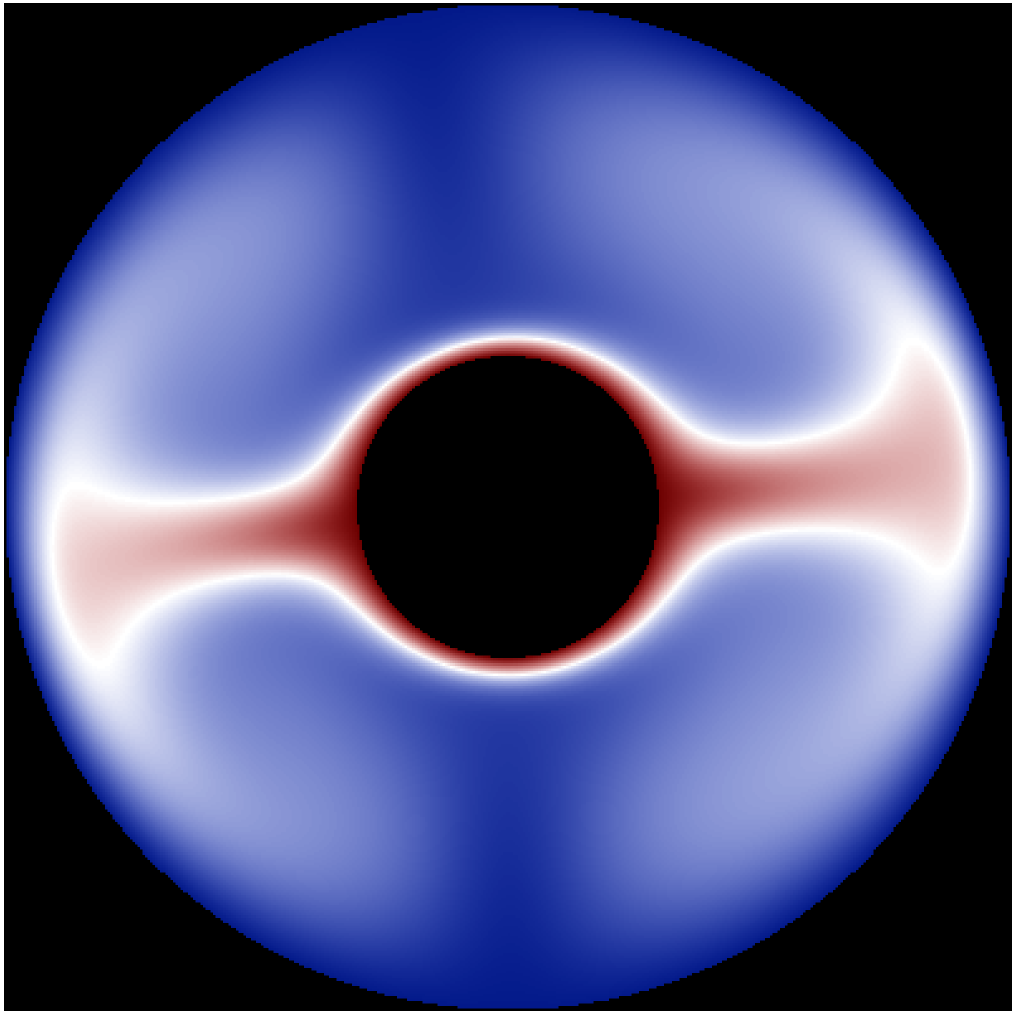

Ra=10^4 Nu=3.5

Figure courtesy of P. van Keken

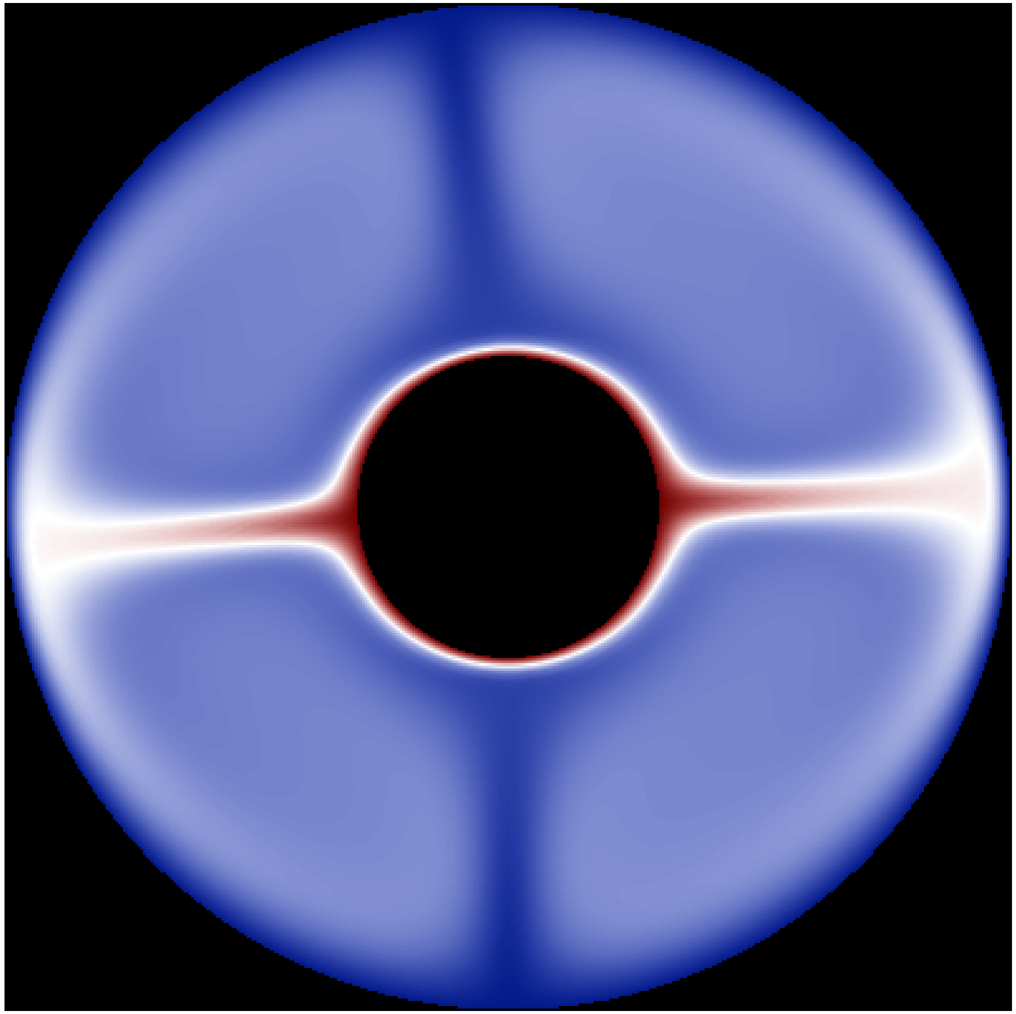

Ra=10^5 Nu=8

Figure courtesy of P. van Keken

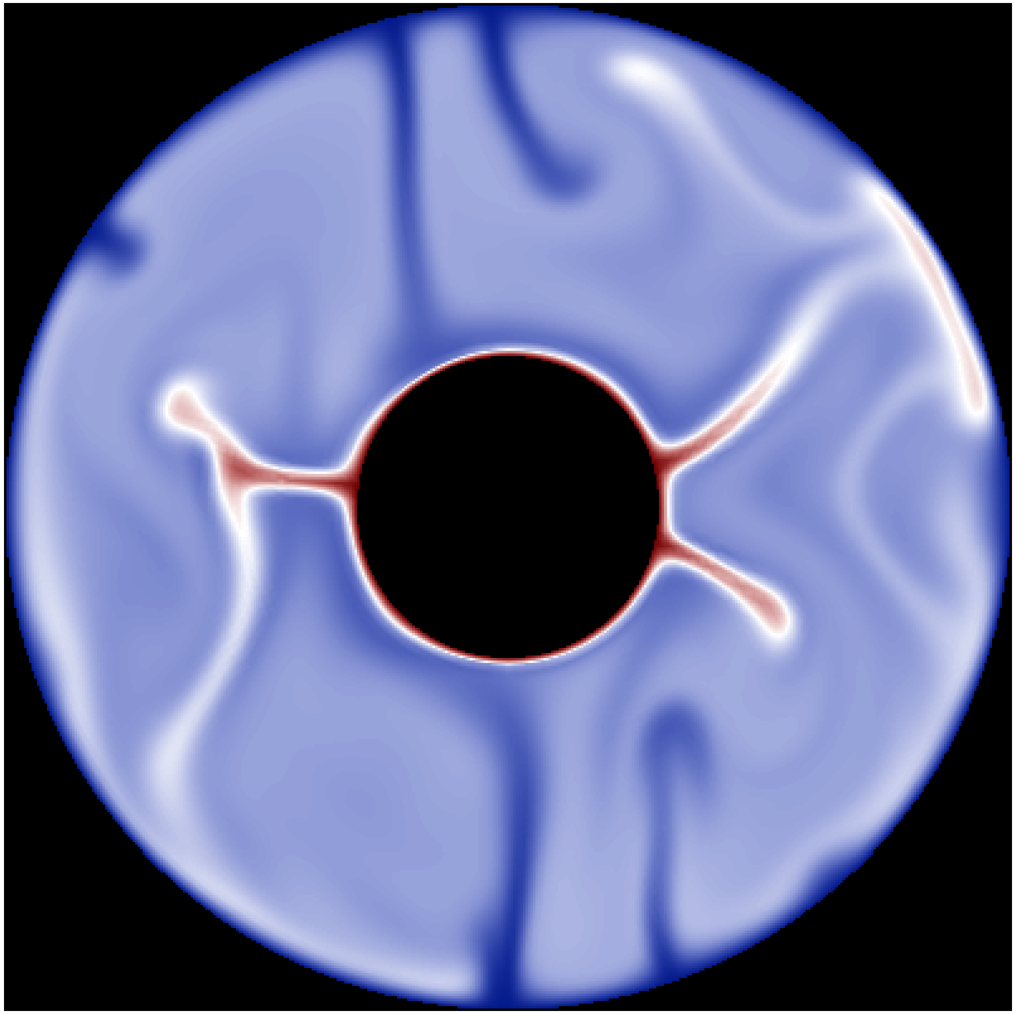

Ra=10^6 <Nu>=16

Figure courtesy of P. van Keken

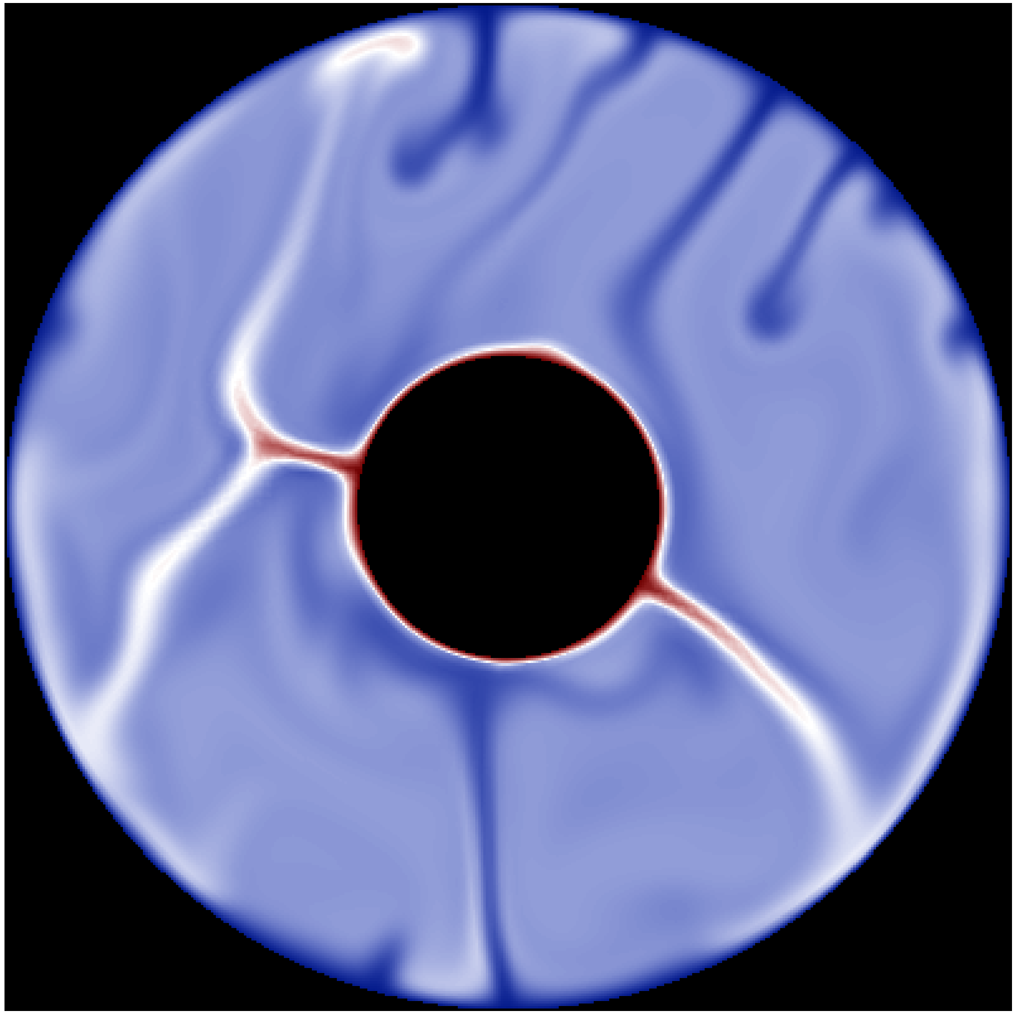

$Ra=2x10^6$ $\langle Nu \rangle=18$

Figure courtesy of P. van Keken

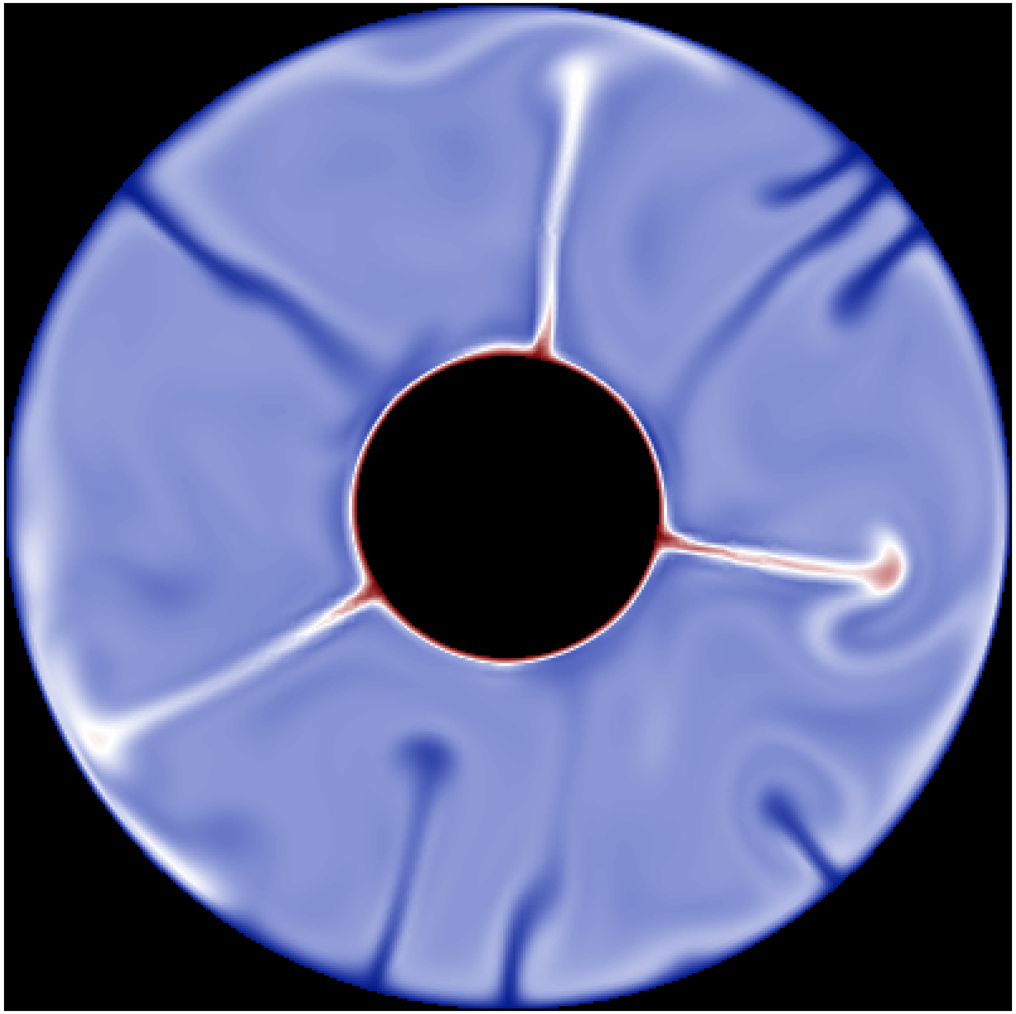

$Ra=5x10^6$ <Nu>=20

Figure courtesy of P. van Keken

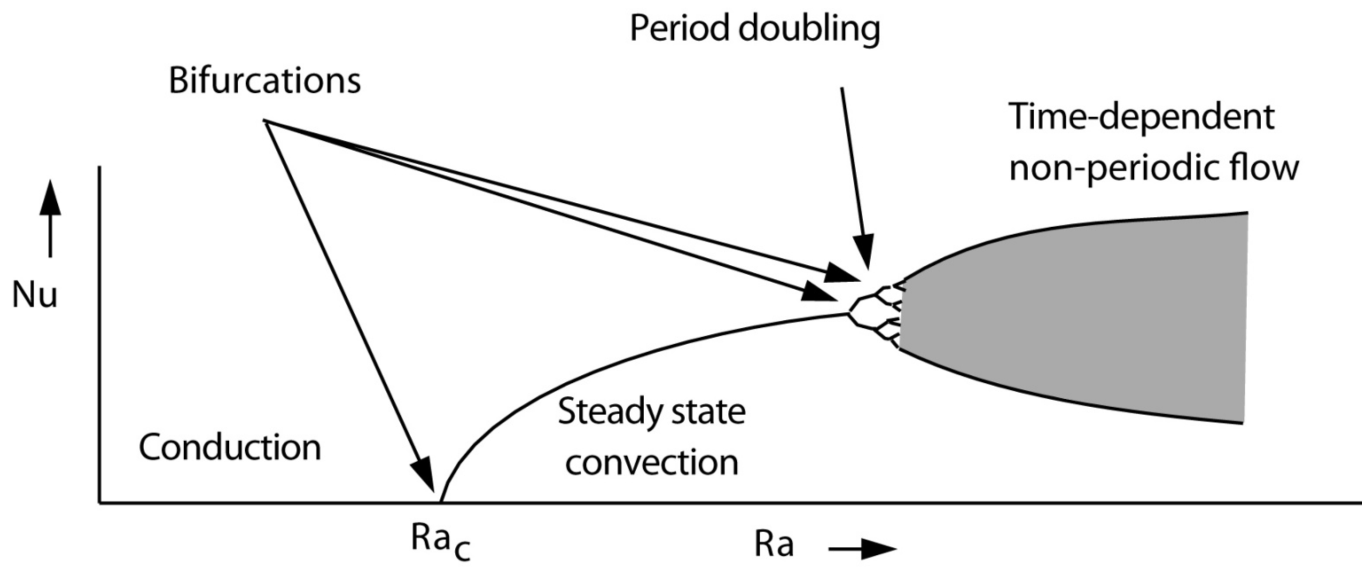

Logistical equation (May, Nature, 1976):

$x_{n+1} = r\, x_n\,(1 – x_n)$

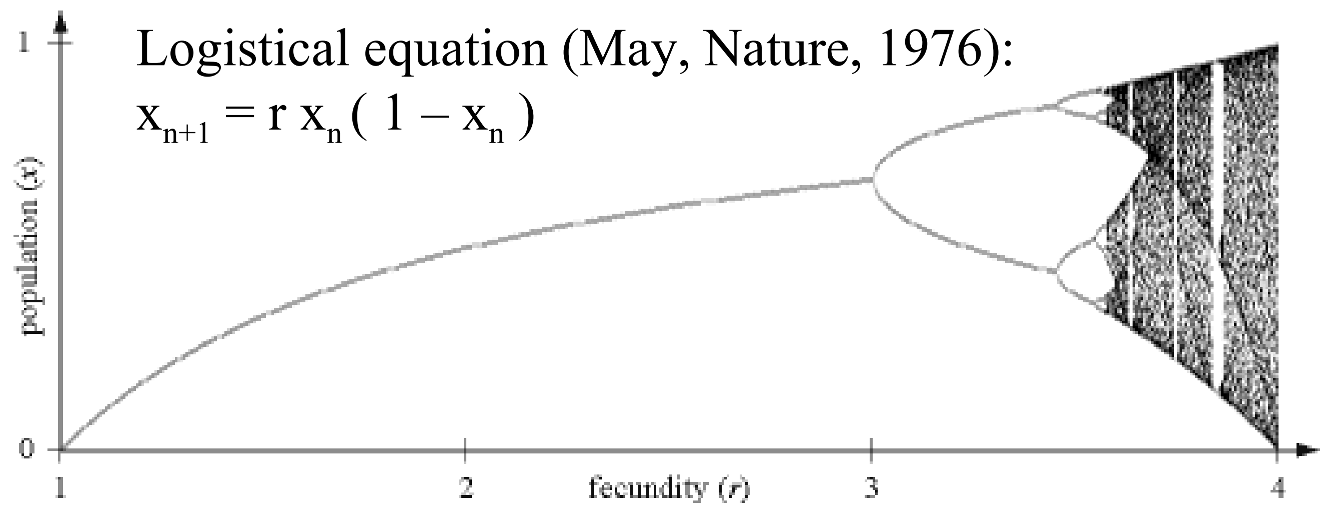

Ra > Ra_c modeling results

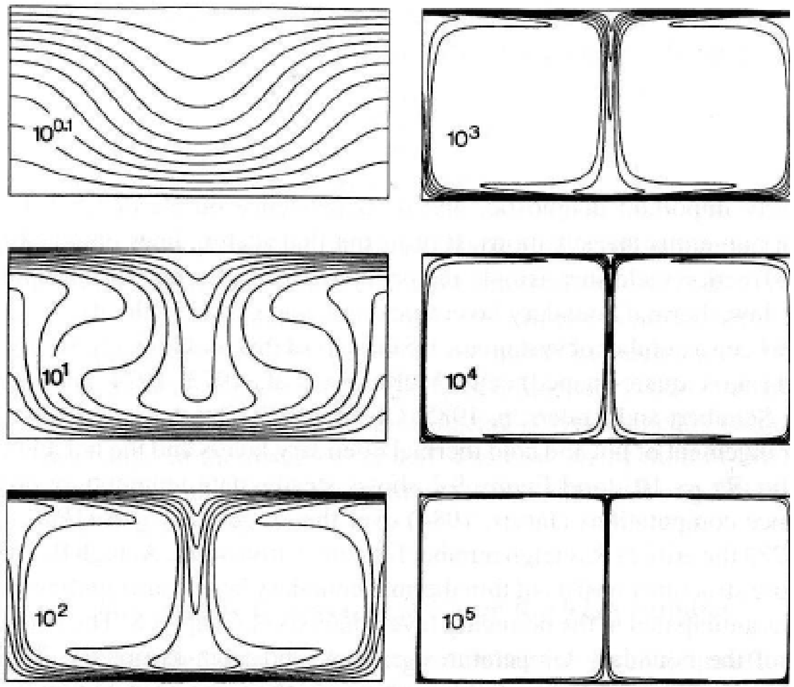

Temperature

Figure 9.2. Contours of temperature for steady, two-dimensional, Rayleigh–Bénard convection in aspect rati one cells heated from below (Jarvis, 1984), showing the development of thermal boundary layers with increasin Rayleigh number. Numbers indicate the ratio Ra/Ra_{cr}, with $Ra_{cr} = 779.27$.

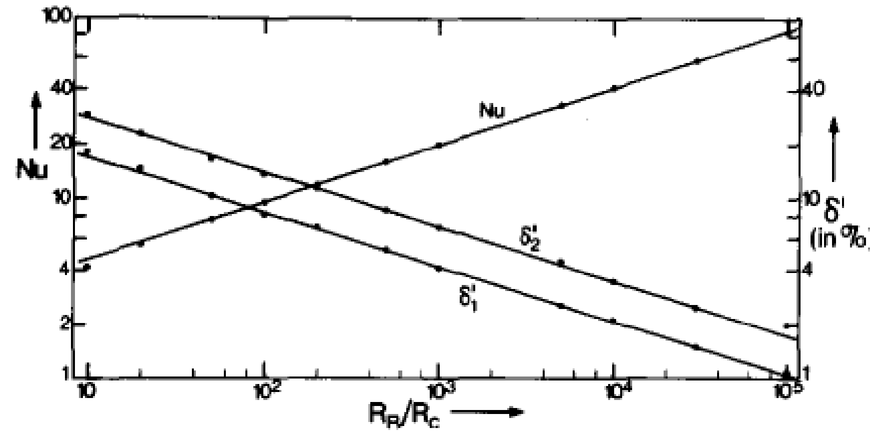

Fig. 3. Plots of Nu, and $\delta'(=\delta/d)$, as functions of R_B/R_c. All values are plotted on logarithmic scales. δ_1' represents the shallowest depth at which the mean temperature $\Delta T/2$ occurs in the mean temperature profile, while δ_2' represents the mean depth of the maximum temperature in the upper thermal boundary layer. The straight lines have been fit through the model predictions for all models with $100 \leqslant R_B/R_c \leqslant 30000$. The data included in these graphs are tabulated in Table I in the Appendix.

- higher Ra gives thinner thermal boundary layers
- For larger Ra flow usually not steady state

2D convection experiments, isoviscous case

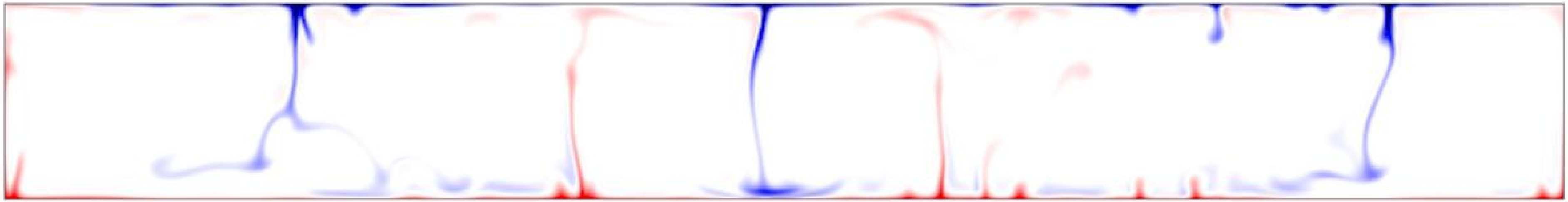

$Ra = 10^7$ $H = 0$ $\eta'(T) = 1$ $\eta_{lm}/\eta_{um} = 1$

Courtesy of Allen McNamara

Temperature dependent viscosity

$Ra = 10^7$ $H = 0$ $\eta'(T) = 1000$ $\eta_{lm}/\eta_{um} = 1$

Courtesy of Allen McNamara

Thermal convection in the mantle

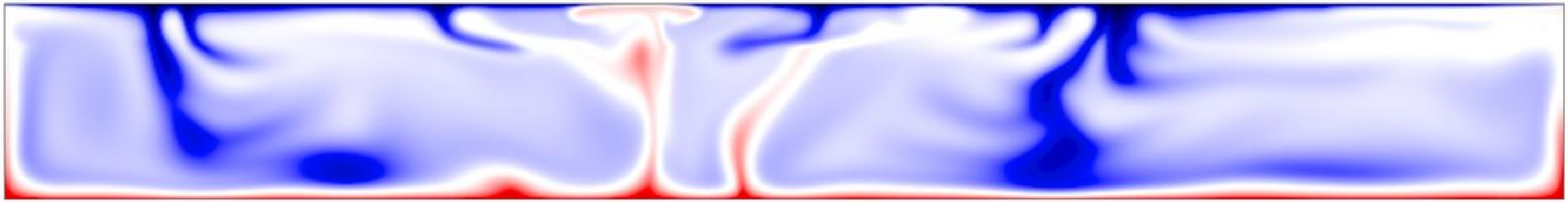

Ra = 10^7 H = 0 $\eta'(T) = 1000$ $\eta_{lm}/\eta_{um} = 50$

Courtesy of Allen McNamara

Increase of internal heating

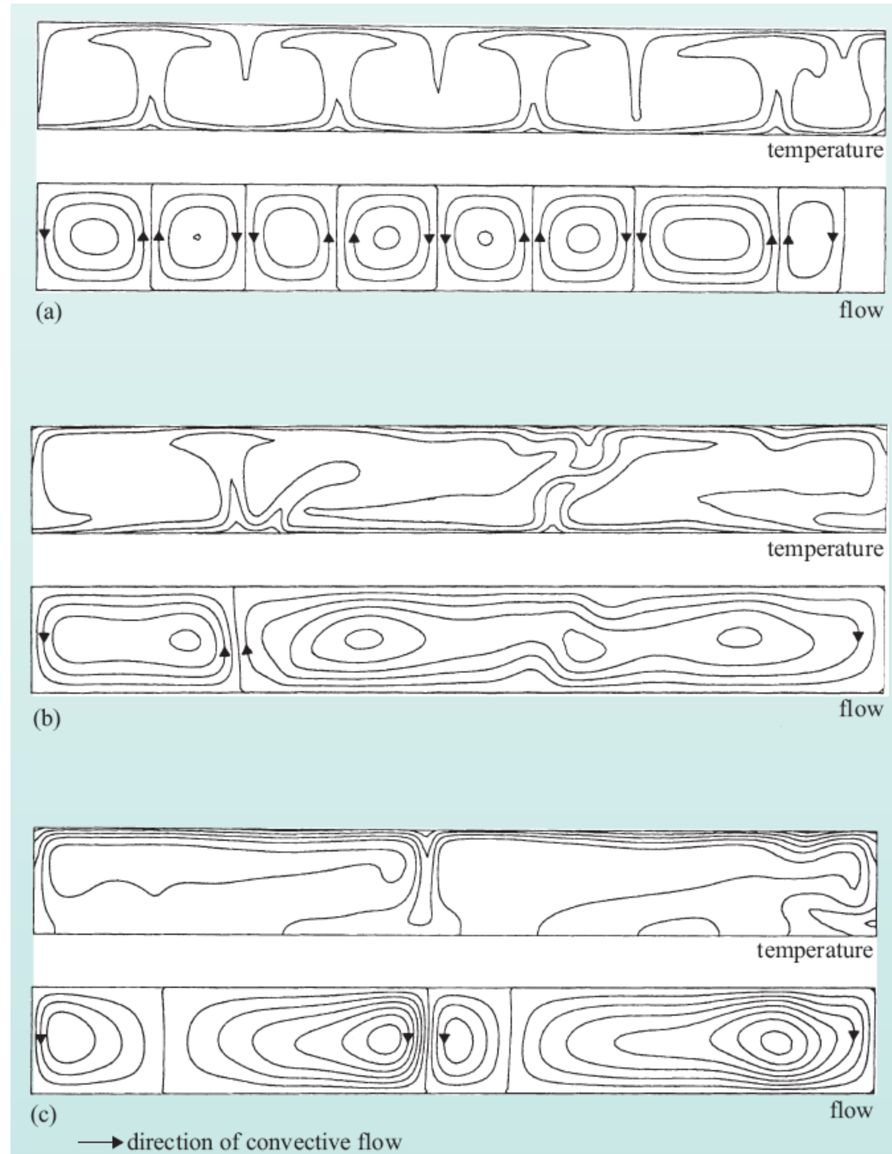

Ra = 2.4e5

Heating mode

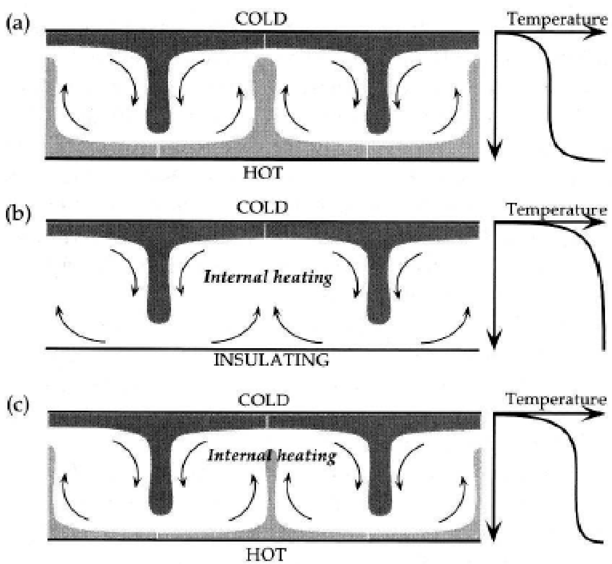

Figure 8.3. Sketches illustrating how the existence and strength of a lower thermal boundary layer depend on the way in which the fluid layer is heated.

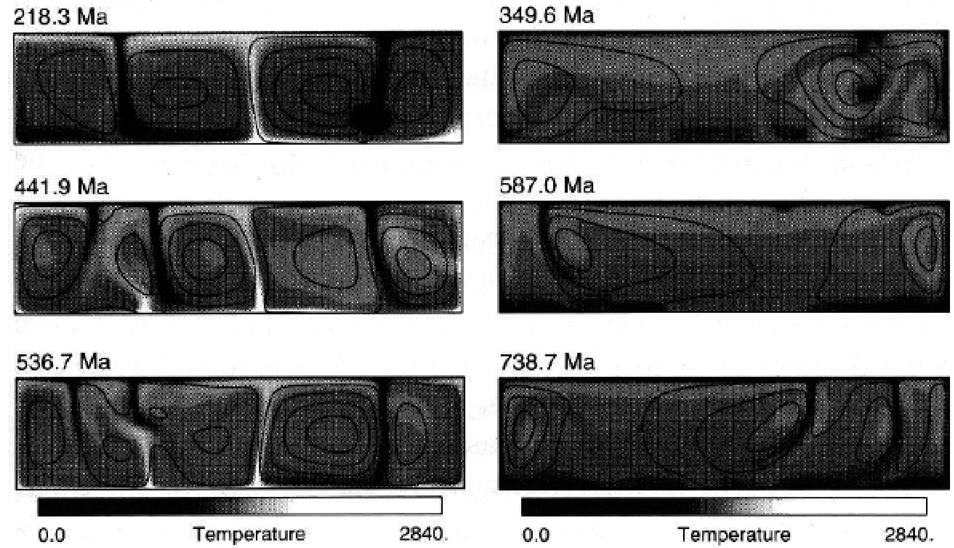

Figure 8.4. Frames from numerical models, illustrating the differences between convection in a layer heated from below (left-hand panels) and in a layer heated internally (right-hand panels). (Technical specifications of these models are given in Appendix 2.)

from (Davies, 1999)

- bottom/internal heating
- passive/active upwellings (MOR?)
- time dependence
- bottom/top boundary layer independent (plumes vs. plates)

Convection with η(T) (1)

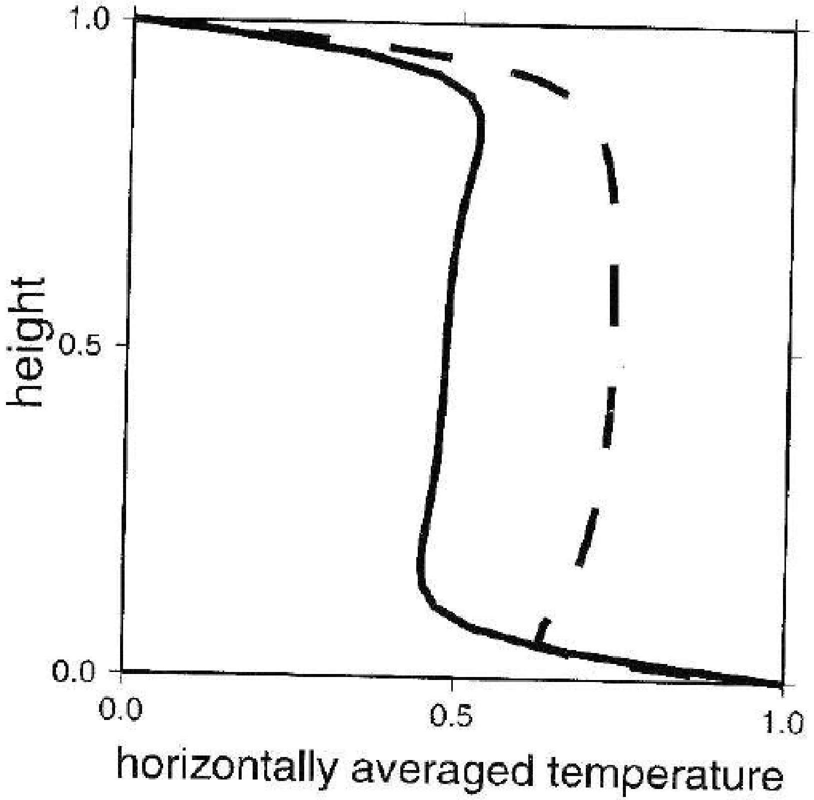

Figure 2. Temperature profiles (i.e., horizontally averaged temperature versus depth) for a basally heated, plane layer of fluid undergoing thermal convection when its viscosity is constant (solid curve) and temperature-dependent (dashed). The profiles show that most of the temperature change across the fluid occurs in relatively narrow *thermal boundary layers* near the top and bottom surfaces. In between the two boundary layers, most of the fluid is stably stratified or (if very well mixed) homogeneous. The fluid with temperature-dependent viscosity develops a stiffer upper thermal boundary layer which acts as a heat plug (i.e., it reduces convection's ability to eliminate heat), causing most of the rest of the fluid to heat up to a larger average temperature. (After Tackley [1996a].)

- large aspect ratios
- large viscosity variations in top 200 km
- asymmetry between up- & downwellings

from Bercovici et al., (1996)

Convection with η(T) (2)

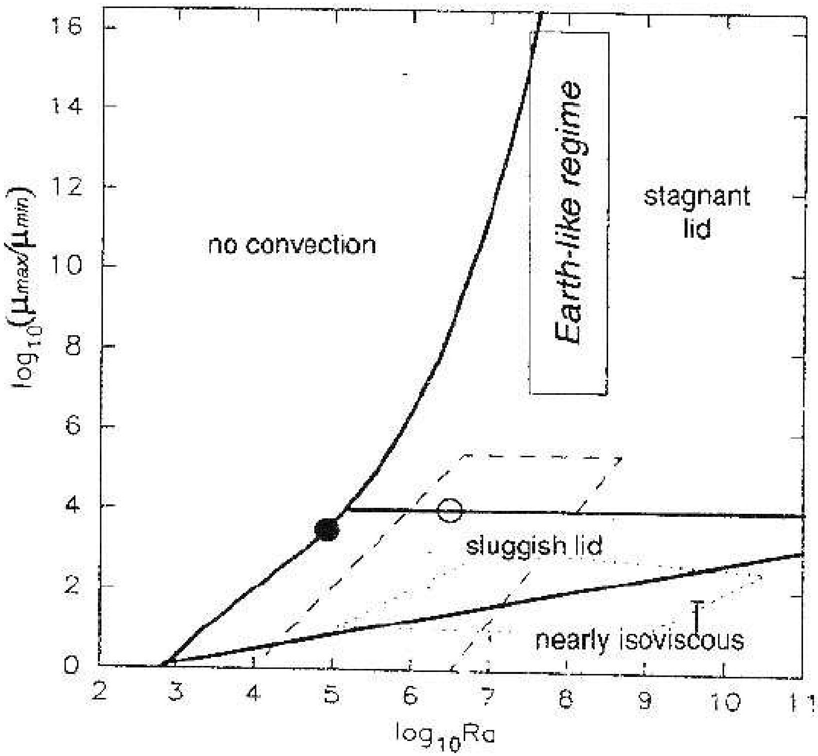

Figure 6. Diagram showing the different convective regimes in "*Ra* versus viscosity ratio" space for convection in fluid with temperature-dependent viscosity; μ_{max} and μ_{min} are the maximum and minimum allowable viscosities of the fluid, respectively. Dashed and dotted boxes show the regime of various numerical convection experiments. The box with the solid boundary shows the likely regime for the Earth. See text for discussion. (After Solomatov [1995].)

Stagnant lid regime on Earth?
→ missing rheology!

from Bercovici et al. (1996)